104 (2025) 104884

Contents lists available at ScienceDirect

Poultry Science

journal homepage: www.elsevier.com/locate/psj

Full-Length Article

Multi-omics analyses reveal that sirtuin 5 promotes the development of pre-recruitment follicles by inhibiting the autophagy-lysosome pathway in chicken granulosa cells

Ruotong Zou [a], Li Wang [b], Xi Zhang [a], Siyao Dong [a], Zhidan Zhang [a], Donghong Chen [a], Lingbin Liu [a], Anfang Liu [a], Felix Kwame Amevor [c], Xi Lan [a,*], Zhifu Cui [a,*]

[a] College of Animal Science and Technology, Southwest University, Beibei, 400715 Chongqing, China
[b] National Center of Technology Innovation for Pigs, Chongqing, China
[c] Farm Animal Genetic Resources Exploration and Innovation Key Laboratory of Sichuan Province, Sichuan Agricultural University, Chengdu 611130, China

ARTICLE INFO

Keywords:
Multi-omics
Follicular pre-recruitment
Sirtuin 5
ROS
Autophagy

ABSTRACT

The development of pre-recruitment follicles plays a critical role in determining egg-laying performance in poultry. This study combines proteomic and metabolomic analyses to explore changes in proteins and metabolites, to elucidate key regulatory mechanism involved in chicken pre-recruitment follicular development. Histological examination revealed a significant increase in yolk deposition in small yellow follicles (SYF) compared to small white follicles (SWF). Metabolomics analysis identified significantly enriched differential metabolites (DMs) between SWF and SYF in pathways such as Lysosome, Ferroptosis, Biosynthesis of unsaturated fatty acids, and Tryptophan metabolism. Particularly, Adenosine-5′-Diphosphate (ADP) was downregulated during follicular recruitment and was significantly enriched in the lysosome pathway. Proteomic analyses revealed that differentially expressed proteins (DEPs) in SWF and SYF were enriched in pathways including Lysosome, Glutathione metabolism, Cholesterol metabolism, Arginine and proline metabolism, and amino acid biosynthesis. Among these DEPs, NAD-dependent protein deacetylase sirtuin 5 (SIRT5) was significantly upregulated, while lysosomal-associated membrane protein 1 (LAMP1) was down-regulated during the development of pre-recruitment follicles. SIRT5 was linked to the negative regulation of reactive oxygen species metabolism, whereas LAMP1 was associated with lysosome and autophagy pathways. Further validation experiments demonstrated high expression of SIRT5 in SYF, particularly in granulosa cells (GCs). Silencing SIRT5 in GCs resulted in increased ROS production and upregulated expression of autophagy-related proteins LC3II and Beclin1, as well as lysosome markers LAMP1. Conversely, lipid droplet deposition and p62 expression were suppressed. inhibited. Taken together, these findings suggest that SIRT5 upregulation promotes the development of pre-recruitment follicles by inhibiting the autophagy-lysosome pathway in chicken GCs.

Introduction

Eggs are a nutrient-dense food source, offering high-quality protein along with essential vitamins, fats, and minerals (Soliman, 2018; Shakoor et al., 2020; Nishio and Isobe, 2023). Addressing global food security challenges has necessitated advancements in egg production to meet the growing demand (Wang et al., 2017a; Guiné, 2024). In poultry, egg production is intricately tied to the orderly development of ovarian follicles. Following sexual maturity, hens exhibit cyclic egg-laying patterns, with ovarian follicles progressing through sequential stages (Johnson et al., 2015). This process involves recruitment, selection, dominance, and maturation of follicles (McGee and Hsueh, 2000; Johnson and Alan, 2014). Ovarian follicles in chickens are organized hierarchically by size, with pre-hierarchical follicles classified as small white follicles (SWF, 2-4 mm), large white follicles (LWF, 4-6 mm), and small yellow follicles (SYF, 6-8 mm). Hierarchical follicles include the fifth (F5), fourth (F4), third (F3), second (F2), and largest preovulatory follicle (F1) (Etches and Petitte, 1990; Onagbesan et al., 2009; Johnson, 2015b). Upon ovulation, a follicle from the pre-hierarchal group is selected to progress into the hierarchical stage (Onagbesan et al., 2009).

* Corresponding authors at: College of Animal Science and Technology, Southwest University, Beibei, 400715 Chongqing, China
E-mail address: cui20221732@swu.edu.cn (Z. Cui).

https://doi.org/10.1016/j.psj.2025.104884
Received 4 December 2024; Accepted 4 February 2025
Available online 7 February 2025

This process, known as follicle selection, involves an SYF advancing to replace the F5 follicle. Before selection, SWF transition into the SYF pool through the development of pre-recruitment follicles (Johnson and Woods, 2009; Johnson, 2015a; Kim and Johnson, 2016; Sasanami, 2017). Small follicles that are not recruited to enter the rapid growth phase undergo atresia, even during the laying phase (Johnson, 2015b). The preovulatory hierarchy is synchronized with the ovulatory cycle, relying on daily selection rhythms that allow specific follicles to progress in growth (Johnson, 2015a). Granulosa cells (GCs), which surround the oocyte, play a pivotal role in regulation of the follicle selection via G protein-coupled receptor-mediated signaling pathways (Johnson, 2015a). Follicle recruitment and selection are key rate-limiting steps in avian reproduction, with low rates indicating potential for significant improvement in laying performance (Johnson, 2015a). Therefore, understanding these underlying mechanisms holds both theoretical and practical importance.

Follicular development is governed by a stringent, complex intrinsic regulatory system (Zhou et al., 2020). During this process, key events such as gene transcription and protein expression occur in a coordinated manner, regulated by specific gene networks that influence follicular recruitment, selection, and atresia (Fiorentino et al., 2023). Follicular atresia, a critical event in ovulatory follicle selection, occurs throughout all developmental stages in poultry (Gilbert et al., 1983). Aging exacerbates follicular atresia and contributes to declining egg production, primarily due to granulosa cell apoptosis (Yu et al., 2004; Hussein, 2005; Rolaki et al., 2005). Recent studies suggests that GCs autophagy complements apoptosis in driving follicular atresia (Dong et al., 2022; Han et al., 2022; He et al., 2022; Shao et al., 2022; Han et al., 2023; He et al., 2024a).

The laying hen (*Gallus gallus domesticus*) is an excellent model for studying ovarian follicle recruitment and selection due to its nearly daily recruitment cycles during the year-long laying period. Over the past decade, high-throughput sequencing technologies have been used to investigate the genetic mechanisms underlying avian follicular development (Li et al., 2022). These studies have explored follicular recruitment (Ocłoń and Hrabia, 2021; Sun et al., 2021; Sun et al., 2022), selection (Wang et al., 2017b; Li et al., 2019; Sun et al., 2021; Sun et al., 2022), and atresia (Yu et al., 2016; He et al., 2022; Yu et al., 2022; Yang et al., 2023). However, limited studies have focused on the key regulatory proteins and metabolites involved in the development of chicken ovarian pre-recruitment follicles. In this present study, we integrated proteomic and metabolomic analyses to identify protein and metabolite changes, aiming to uncover the crucial regulatory mechanism underlying follicular recruitment in chickens.

Materials and methods

Animals and sample collection

In this study, a total of 360 Nanchuan chickens (Chinese local chicken breed) at 280 days old were raised under standard management conditions and water provided *ad libitum*. Twelve chickens were randomly selected and euthanized for the collection of follicles such as pre-hierarchical follicles [small white follicle (SWF), large white follicle (LWF), small yellow follicle (SYF)] and hierarchical follicles [the fifth (F5), fourth (F4), third (F3), second (F2), and largest preovulatory follicle (F1)]. Follicle classification followed the method described by Onagbesan (Onagbesan et al., 2009). All the SWF and SYF samples were immediately placed into sample tubes, wrapped in foil, snap-frozen in liquid nitrogen, and stored at −80 °C for further analyses. The animal experiments were approved by the Institutional Animal Care and Use Committee of Southwest University (Certification No. LAC2023-2-0058). All experiments were conducted in accordance with the Laboratory Animal Welfare and Ethics guidelines.

Hematoxylin and Eosin (H&E) staining

The Hematoxylin and Eosin (H&E) staining of the follicular tissues were performed following previously established protocols (Cui et al., 2022). Briefly, the SWF and SYF tissues were fixed in 4 % paraformaldehyde for 24 h, dehydrated in graded ethanol concentrations, embedded in paraffin, and sectioned into 3-5 μm slices. The tissue sections were mounted on slides, stained with H&E, sealed with neutral resin, and imaged using a TEM JEM-1400 microscope (JEOL, Tokyo, Japan) with an AMT CDD camera (Sony, Tokyo, Japan).

Protein extraction and quality control

Protein extraction and quality control were conducted as described previously (Cui et al., 2022). Briefly, appropriate samples were weighed, mixed with 1 × Cocktail, and placed on ice for 5 min before addition 10 mM DTT. The tissues were then ground and centrifuged to collect the supernatant. The solution was treated with 10 mM DTT and incubated in a water bath at 56 °C for 1 h. Subsequently, 55 mM IAM was added, and the samples were incubated in the dark for 45 min. Thereafter, cold acetone (1:5) was added, and the mixture was stored at -20 °C for 30 min. After the centrifugation at 4 °C (25,000 × g, 15 min), the precipitate was air-dried and resuspended in lysis buffer. A second centrifugation was performed to collect the protein-containing supernatant. Further, protein quality control was assessed using Bradford quantification and SDS-PAGE.

DDA and DIA analysis by nano-LC-MS/MS

Data dependent acquisition (DDA) and data independent acquisition (DIA) analyses were performed using nano-LC-MS/MS following previously described methods (Cui et al., 2022). DDA fractions were analyzed using a Q-Exactive HF mass spectrometer (Thermo Fisher Scientific, San Jose, CA) coupled with an Ultimate 3000 RSLCnano system (Thermo Fisher Scientific).

Metabolite extraction and non-targeted LC-MS/MS metabolomics analysis

Metabolite extraction and non-targeted LC-MS/MS analysis were performed as described previously (Cui et al., 2022). Follicle tissues (100 mg) were ground in liquid nitrogen, resuspended in pre-chilled 80 % methanol, and vortexed thoroughly. Samples were incubated on ice for 5 min and centrifuged at 15,000 × g at 4 °C for 20 min. Briefly, (1) 100 mg follicle tissues were grounded in liquid nitrogen, resuspended in prechilled 80 % methanol, by thorough vortexing; (2) all the 18 follicular tissue samples were incubated on ice for 5 min and centrifuged at 15,000 × g, 4 °C for 20 min; (3) the supernatant samples were diluted to final concentration containing 53 % methanol by LC-MS grade water; (4) the samples were subsequently transferred to a fresh Eppendorf tube and then were centrifuged at 15,000 × g, 4 °C for 20 min, and finally, the supernatant was injected into the LC-MS/MS system for analysis (Want et al., 2013). In this present study, a Waters 2D UPLC (Waters, USA) tandem Q Exactive high resolution mass spectrometer (Thermo Fisher Scientific) was used for metabolite separation and detection. Then the data from the primary and secondary mass spectrometry were collected using Q Exactive mass spectrometer (Thermo Fisher Scientific).

Bioinformatic analysis

Protein and genome annotation were conducted using the UniProt and RefSeq databases. In this study, MaxQuant (http://www.maxquant.org) software was used for DDA data identification, which served as a spectral library for subsequent DIA analysis (Cox and Mann, 2008), using Spectronaut software (version 18.4) (Bruderer et al., 2015). R package MSstats (version 4.0.1) (Choi et al., 2014) was used for statistical evaluation of significant differences in proteins or peptides from

Table 1
Oligonucleotide sequences of SIRT5 interfering vectors.

Name	Sense 5′-3′	Antisense 5′-3′
gga SIRT5-219	CCGAGAAGUGUUUGCCAAATT	UUUGGCAAACACUUCUCGGTT
gga SIRT5-407	GCGAGGUCAUGCUGAGUAATT	UUACUCAGCAUGACCUCGCTT
gga SIRT5-598	GGAAACGUGACUGCAAAUUTT	AAUUUGCAGUCACGUUUCCTT

different samples. Thereafter, we performed differentially expressed proteins (DEPs) screening based on a fold change ≥ 2 and adj_P-value < 0.05 as the criteria for a significant difference. Differential metabolites (DMs) were identified using VIP (VIP > 1) and P-value (P-value < 0.05, Student's t test) with VIP values obtained from OPLS-DA analysis which also contained score plots and permutation plots, using the MetaboAnalystR package (version 4.0). The data was log transform (log2) and mean centered before OPLS-DA. Identified DEPs and DMs were annotated using KEGG Compound database (http://www.kegg.jp/kegg/compound/), annotated DEPs and DMs were mapped to KEGG Pathway database (http://www.kegg.jp/kegg/pathway.html), with pathway enrichment assessed via hypergeometric testing (P-value for a given list of DEPs and DMs).

Cell culture, identification, and transfection

The small yellow follicles were collected and processed in sterile Hank's balanced salt solution. Primary GCs were isolated following the methods previously described (Gilbert et al., 1977), using β-II collagenase (BaiTai Biotechnology, Chengdu, China) and filtered through 200-mesh cell sieves. Thereafter, it was resuspended in Dulbecco's modified Eagle medium (DMEM) + 10 % fetal bovine serum (Gibco, Grand Island, NY, United States) + 0.1 % mixture of penicillin-streptomycin (Invitrogen, Carlsbad, CA, United States). Thereafter, the GCs were cultured in an incubator at 37 °C, 5 % CO_2, and 95 % air saturated humidity and the media changed every 24 h. When the confluence of the GCs reached 70∼80 %, the transfection procedure was performed with small interfering RNA (siRNA) using lipofectamine 3,000 reagent (Invitrogen, United States) according to the manufacturer's instructions. Three siRNAs (si-SIRT5-219, si-SIRT5-407, and si-SIRT5-598) were used to knockdown SIRT5 expressions. Oligonucleotide sequences are listed in Table 1.

Immunofluorescence analysis

SWF and SYF tissues were fixed in 4 % paraformaldehyde at room temperature (RT) for 12h and placed in 20 % sucrose solution overnight. Thereafter, the tissue was embedded in paraffin, cut into thin slices (3-5 μm) and placed on a slide. After which they were treated with hydrogen peroxide solution (3 %) to deactivate the endogenous enzymes. Subsequently, the samples were washed with PBS solution for 5 min, and then a blocking reagent (goat serum) was added at RT for 20 min after which they were incubated with primary antibodies overnight at 4 °C. After incubation, the samples were washed and incubated with fluorescence-labeled secondary antibody at RT for 30 min. After the second incubation, the samples were further washed in PBS and incubated for the third time with peroxidase (POD)-labeled streptavidin (DyLight 488) at RT for 30 min. A DAB kit (BBI, Canada) was used for color development at RT for 5 ∼ 30 min, which was followed by observation, and photomicrographs were obtained using a light microscope (Nikon Eclipse E100, Japan) equipped with an imaging system (Nikon DS-U3, Japan). Follicle-stimulating hormone (FSHR) immunofluorescence assay was performed to identify GCs following established protocols. (He et al., 2022). The cells were placed in a 6-well plate and washed with PBS for 5min. Subsequently, the cells were fixed in 4 % paraformaldehyde for 10 min and washed again, and 0.2 % Triton X-100 were added to ensure permeability of the cell membrane for 10 min. The cells were washed and subsequently incubated overnight at 4 °C with primary antibodies. The next morning, the cells were washed and incubated with fluorescence-labeled secondary antibodies at room temperature for 1h. Cells were finally washed in Tris-Buffered Saline Tween-20 (TBST) and florescence intensity was observed and analyzed using a fluorescence microscope (DP80; Olympus, Japan). The images obtained were analyzed using Image-Pro Plus software (version 6.0, Media Cybernetics, Silver Spring, USA).

Oil red O staining

Oil Red O staining was performed on GCs to assess lipid accumulation (Cui et al., 2022; Ning et al., 2023). Briefly, GCs were washed in a phosphate buffered saline (PBS) and fixed with ORO Fixative (Solarbio, Beijing, China) for 30 min, the stationary fluid was discarded and then washed twice in PBS. After that, 60 % isopropanol was added and maintained for 5 min, and Oil Red O (Solarbio) was added and retained for 20 min. Furthermore, Mayer Hematoxylin staining solution (Solarbio) was added and incubated for 2 min after the GCs were washed 5 times. Moreover, the ORO (Solarbio) was added and sustained for 1 min. After washing with PBS, the distilled water was used to cover the GCs. All the sections and GCs were viewed under the electronic microscope (DP80Digital, Olympus, Tokyo, Japan), and then ten fields were randomly selected for statistical analysis.

Mitochondrial reactive oxygen species (ROS) Assay

Mitochondrial ROS levels were measured using 2, 7-Dichlorofluorescin (DCFH-DA; Sigma, USA) at a final concentration of 10 μM for 20 min at room temperature. Fluorescence was recorded using a Shimadzu RF-3501 spectrophotometer (Shimadzu, Korneuburg, Austria) at an excitation wavelength of 488 nm and an emission wavelength of 525 nm.

Quantitative real-time reverse transcription-polymerase chain reaction (qRT-PCR)

Total RNA was extracted from all the samples using TRIzol reagent (Molecular Research Center, Cincinnati, OH, USA), and RNA concentration and purity were assessed using the A260/A280 absorbance ratio, and the 18 S and 28 S bands in a 1 % agarose gel. Reverse transcription and qRT-PCR were performed as previously described (Cui et al.,

Table 2
Primers used for qRT-PCR.

Gene	Sequence (5′-3′)	Product Length (bp)	Annealing Temperature (°C)	Accession Number
ATG5	F:AAGCAACTGTGGATGGGGTT R:GGTGTTTCCAGCATTGGCTC	299	59	XM_046914034.1
ATG7	F:CCAGGGGATTCTACCAGGGA R:CGCAAGAGCTCCAGCTATCA	87	60	NM_001396469.1
SIRT5	F:CTATGCGACCTCTGCTTGGT R:CCTGAACCTGTCTGTAGCGG	138	60	NM_001276364.2
*GAPDH**	F:TCCTCCACCTTTGATGCG R: GTGCCTGGCTCACTCCTT	144	60	NM_204305.1

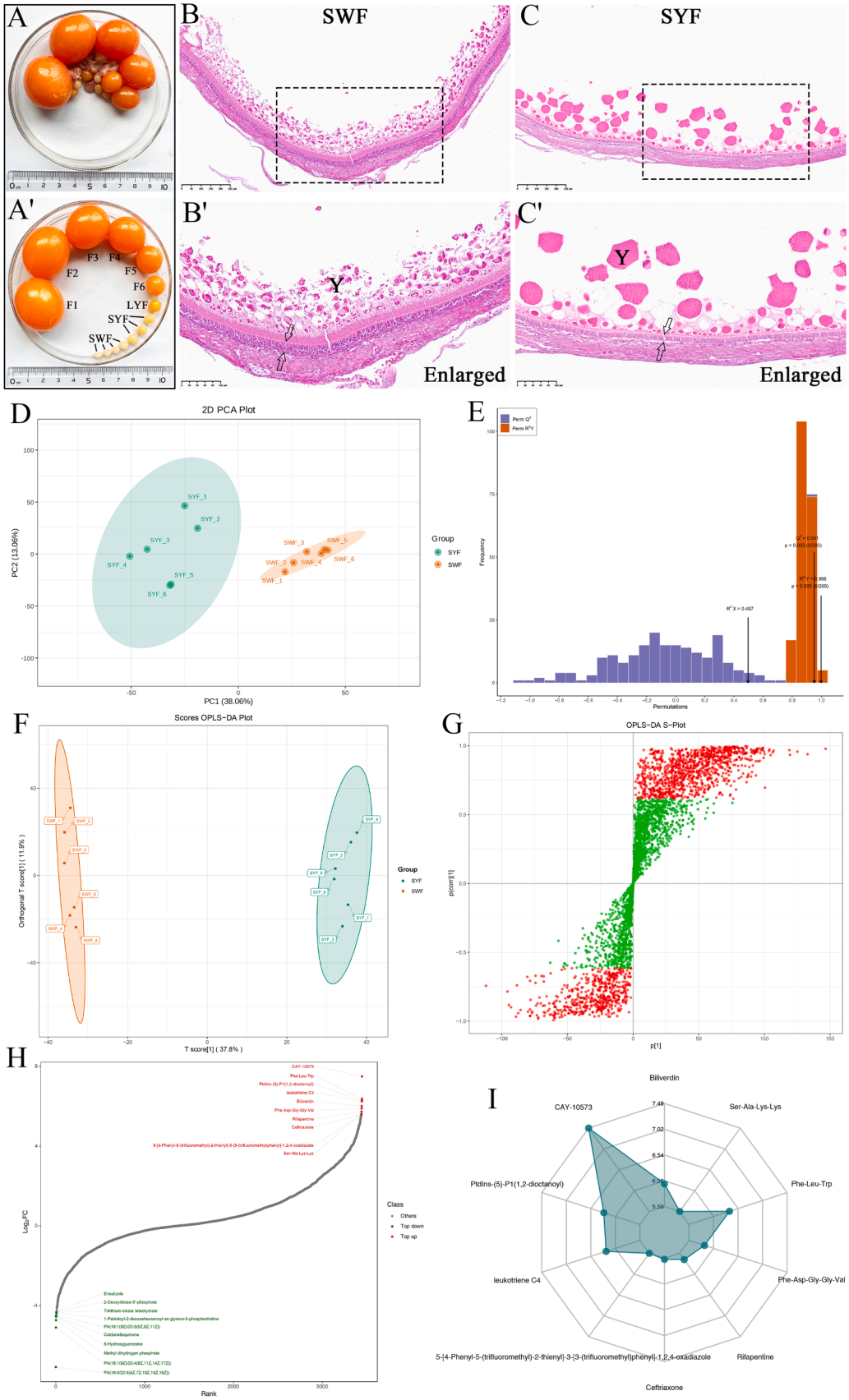

Fig. 1. Comparison of morphology and histological characteristics, and metabolomics analysis of chicken SYF and SWF follicles. (A and A') The morphology characteristics of chicken ovary follicles. (B and B') The histological characteristics of SWF and SYF (C and C'). Y: Yolk. The black arrow indicates the "granular layer". (D) PCA analysis. (E) The validatory results of the OPLS-DA model. (F) The score of OPLS-DA plot. (G) The S-plot of OPLS-DA showed the significantly

different metabolites. (H) The dynamic distribution map of metabolite content differences. (I) The radar map showed the top 10 metabolites with the largest | log_2FC| value.

2020a), using *GAPDH* as the endogenous controls to normalize the gene expression using the $2^{-\Delta\Delta Ct}$ method (Livak and Schmittgen, 2001). The gene-specific primers were designed using Primer Premier 5.0 software according to the coding sequences of target genes and are summarized in Table 2.

Protein extraction and western blot analysis

Further proteins were extracted from the GCs using protein extraction kit (BestBio Biotech Co. Ltd., Shanghai, China), and the BCA protein assay kit (BestBio) was used to determine the concentration of protein samples. Western blot was performed following the method described previously (Cui et al., 2020b; Cui et al., 2021), using the following primary antibodies: anti-SIRT5 [(catalogue no. #8779, Cell Signaling Technology (CST), United States], anti-LC3 (#4108, CST), Anti-LAMP1 (ab25630, Abcam, Cambridge, UK) anti-Beclin-1 (Santa Cruz, Heidelberg, Germany), anti-p62 (#88588, CST). Secondary antibodies: goat anti-mouse (1:5000, 511103, Zen-Bio, Chengdu, China) and goat anti-rabbit (1:5000, 511203, Zen-Bio). The β-Actin (1:1000, 200068, Zen-Bio) was used as a reference.

Statistical analysis

The statistical analysis was conducted with SAS 9.3 software (SAS Institute Inc., Cary, NC, USA). The experimental data were first tested by normal distribution, an unpaired Student's t-test was used for the two-group comparison analysis, with statistical significance indicated as $^*P < 0.05$, $^{**}P < 0.01$, and $^{***}P < 0.001$. All the experimental data were presented as mean ± standard error (SE).

Results

Morphological and histological characteristics, and metabolomics analysis of chicken ovary follicles

Morphological analysis of the chicken ovary revealed the presence of numerous hierarchical follicles and prehierarchical follicles (Fig. 1A and A'). Histological examination through H&E staining showed that GCs in the follicles appeared cuboidal and exhibited significant yolk deposition, with the granulosa layer transitioned from a multi-layered to a single-cell layer during the development of SWF (Fig. 1B and B') to SYF (Fig. 1C and C'). Further, metabolomic analysis of SWF and SYF identified differential metabolites (DMs). The quality of the data was evaluated through the repeatability of QC sample tests in LC-MS/MS negative and positive ion modes. Principal component analysis (PCA) demonstrated that biological replicates are clustered together, with clear separation between different groups (Fig. 1D). An orthogonal partial least squares-discriminant analysis (OPLS-DA) model was used to analyze the metabolome data, and the OPLS-DA validation results confirmed model stability (Fig. 1F; Fig. 1E) The S-plot from OPLS-DA (Fig. 1G) highlighted metabolites with significant differences, located near the upper right and lower left corners. The top 10 upregulated and downregulated metabolites were displayed in a dynamic distribution map (Fig. 1H), and the top 10 metabolites with the largest log2 fold changes (|log2FC|) value were selected and mapped as a radar plot (Fig. 1I). Volcano plots illustrated the relative content differences between the two sample groups, showing 948 significantly upregulated DMs and 487 downregulated DMs in the comparison between SYF and SWF (Fig. 2A). Hierarchical clustering analysis revealed sample similarity, with samples within the same cluster showing greater resemblance (Fig. 2B). To visualize metabolite content changes, Unit Variance Scaling (UV) was applied, and a heatmap was generated using R software (Fig. 2C). Data distribution and its probability density of DMs were shown as Violin diagram (Fig. S1). The metabolites with significant differences were analyzed by Pearson correlation analysis method, and the correlation heat map and chord diagram of DMs were shown as Fig. 2E and Fig. 2F, respectively. KEGG pathway enrichment analysis identified the top 20 enriched pathways by P-value (Fig. 2D), which indicated that DMs were significantly enriched in pathways such as Biosynthesis of cofactors, Purine metabolism, Amino sugar and nucleotide sugar metabolism, Biosynthesis of nucleotide sugars, Tyrosine metabolism, One carbon pool by folate, Ubiquinone and other terpenoid-quinone biosynthesis, Nucleotide metabolism, Lysosome, Ferroptosis, Aminoacyl-tRNA biosynthesis, Insulin signaling pathway, Biosynthesis of unsaturated fatty acids, Tryptophan metabolism among others (Fig. 2D). During follicular recruitment, 2 DMs Adenosine 5′-Diphosphate (ADP) and D-Mannose 6-phosphate were downregulated, which showed significant enrichment in the Lysosome pathway while in the ferroptosis pathway, 6 DMs (Oxiglutatione, Glutathione, Glutathione Reducedform, Arachidonic acid, and Adrenic acid) were downregulated, while γ-Glutamylcysteine was upregulated. The relative abundances of Adenosine 5′-Diphosphate (Fig. 3A), D-Mannose 6-phosphate (Fig. 3B), Oxiglutatione (Fig. 3C), Glutathione (Fig. 3D), γ-Glutamylcysteine (Fig. 3E), Glutathione Reducedform (Fig. 3F), Arachidonic acid (Fig. 3G), Adrenic acid (Fig. 3H) in SWF and SYF are shown in Fig. 3.

Proteomic analyses of SWF and SYF

Proteomic analyses of SWF and SYF showed a separation trend between the groups, with no outliers detected in principal component analysis (PCA) (Fig. 4A). A total of 1276 differentially expressed proteins (DEPs) were identified, including 48 up-regulated and 1228 downregulated proteins (Fig. 4B). Hierarchical clustering analysis of DEPs is shown in a heatmap (Fig. 4C). Gene ontology (GO) analysis revealed that DEPs were involved in several biological processes (BPs) such as cellular processes, metabolic processes, regulation of biological processes, cellular component organismal processes, and other biological functions (Fig. 4D). Pathway classification annotation statistical map of DEPs was shown in Fig. 4E. Top 20 significantly changed pathways associated with DEPs shown in Fig. 3F. The results showed that DEPs were significantly enriched in Metabolic pathways, Cysteine and methionine metabolism, Lysosome, Glutathione metabolism, Cholesterol metabolism, Purine metabolism, Vitamin digestion and absorption, Arginine and proline metabolism, Biosynthesis of amino acids, Endocytosis, Glycolysis/Gluconeogenesis, among others (Fig. 4F). The pathway relationship networks and KOG annotation of DEPs are shown in Fig. 5A and 5B, respectively. In addition, the top 20 highly and differentially expressed proteins were shown in the hierarchical clustering heatmap (Fig. 5C), and the SanKey plot showed the GO and KEGG analysis of these 20 proteins (Fig. 5D).

The expression verification of up-regulated SIRT5 in SWF, SYF, and GCs

Proteomic analyses of the SWF and SYF revealed that NAD-dependent protein deacetylase sirtuin 5 (SIRT5) was significantly upregulated, while lysosomal-associated membrane protein 1 (LAMP1) was down-regulated during the development of pre-recruitment follicles, with SIRT5 involved in the negative regulation of reactive oxygen species metabolism and LAMP1 enriched in lysosome and autophagy pathways (Fig. 5C and D). Subsequently, the H&E staining was carried out to observe the histological characteristics of SYF and SWF (Fig. 6A), and the results showed that during the growth of white follicles, the granulosa layer structure changes from a multi-layer to a single-cell

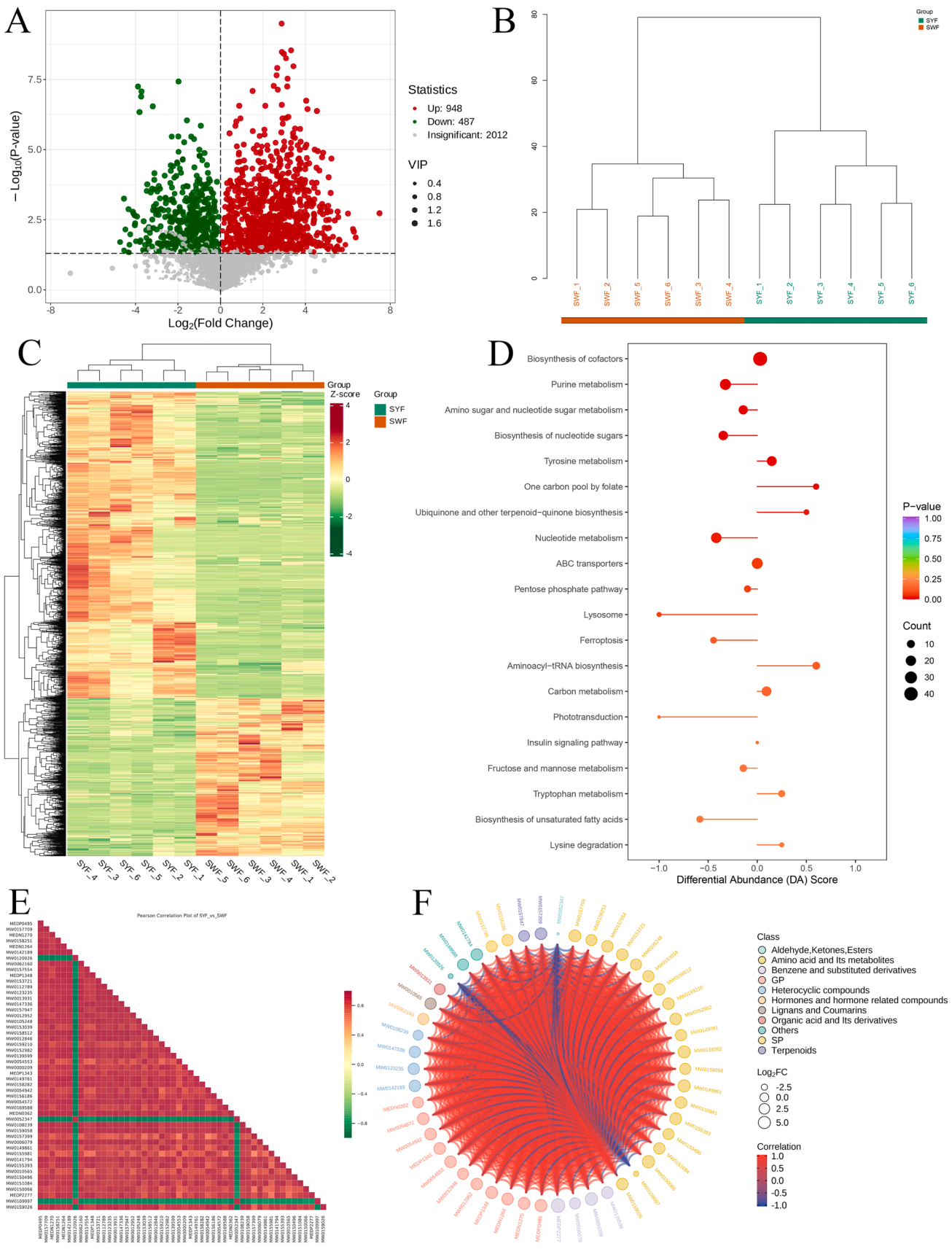

Fig. 2. Functional enrichment analysis of the DMs. (A) Volcano plot showed the DMs in the comparison of SYF and SWF. (B) Hierarchical cluster tree analysis. (C) Hierarchical cluster analysis of DMs. (D) KEGG enrichment analysis of DMs. (E) Pearson correlation analysis of DMs, correlation heat map and (F) chord diagram of DMs.

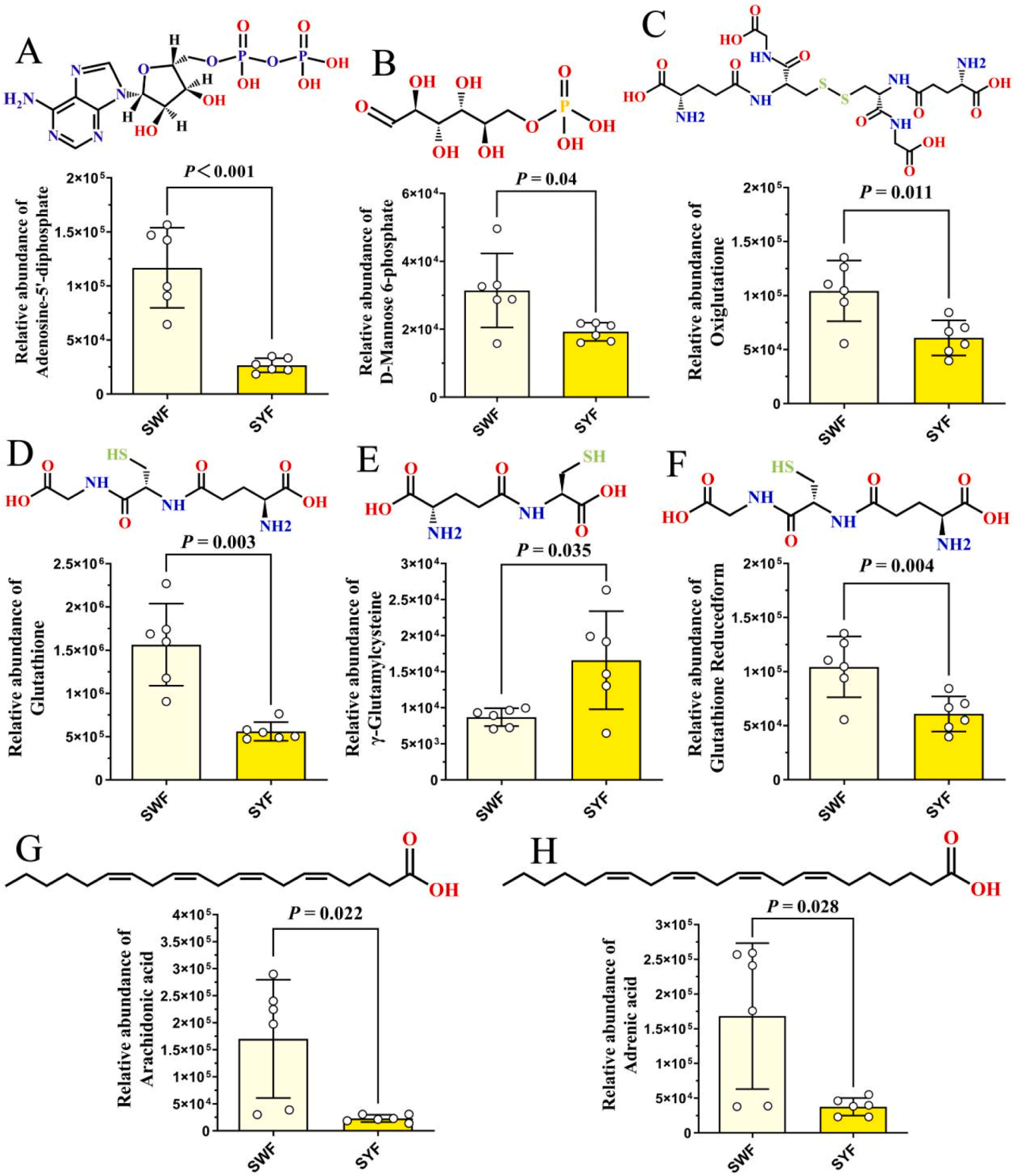

Fig. 3. The abundance of DMs enriched in the Lysosome and Ferroptosis pathways. (A) Relative abundance of Adenosine 5′-Diphosphate, (B) D-Mannose 6-phosphate, (C) Oxiglutatione, (D) Glutathione, (E) γ-Glutamylcysteine, (F) Glutathione Reducedform, (G) Arachidonic acid, (H) Adrenic acid in the SWF and SYF.

layer and the granulosa cells change from an oval shape to a cuboidal shape. The SIRT5 protein expression level in SYF and SWF was detected by immunofluorescence analysis. The results showed that SIRT5 protein expression in SYF was higher than that in SWF (Fig. 6B). Moreover, the mRNA expression of SIRT5 was significantly higher in SYF compared to SWF (Fig. 6C) and was more abundant in granulosa layer than in the theca layer (Fig. 6D). The chicken primary GCs of the follicles were isolated and FSHR immunofluorescence assay was performed to identify the GCs. The results showed that the FSHR was highly expressed in the cell and mainly expressed in cytoplasm, indicating that the cultured cells were GCs (Fig. 6E). Therefore, the immunofluorescence assay of SIRT5 was carried out to detect the protein expression level of SIRT5 in GCs,

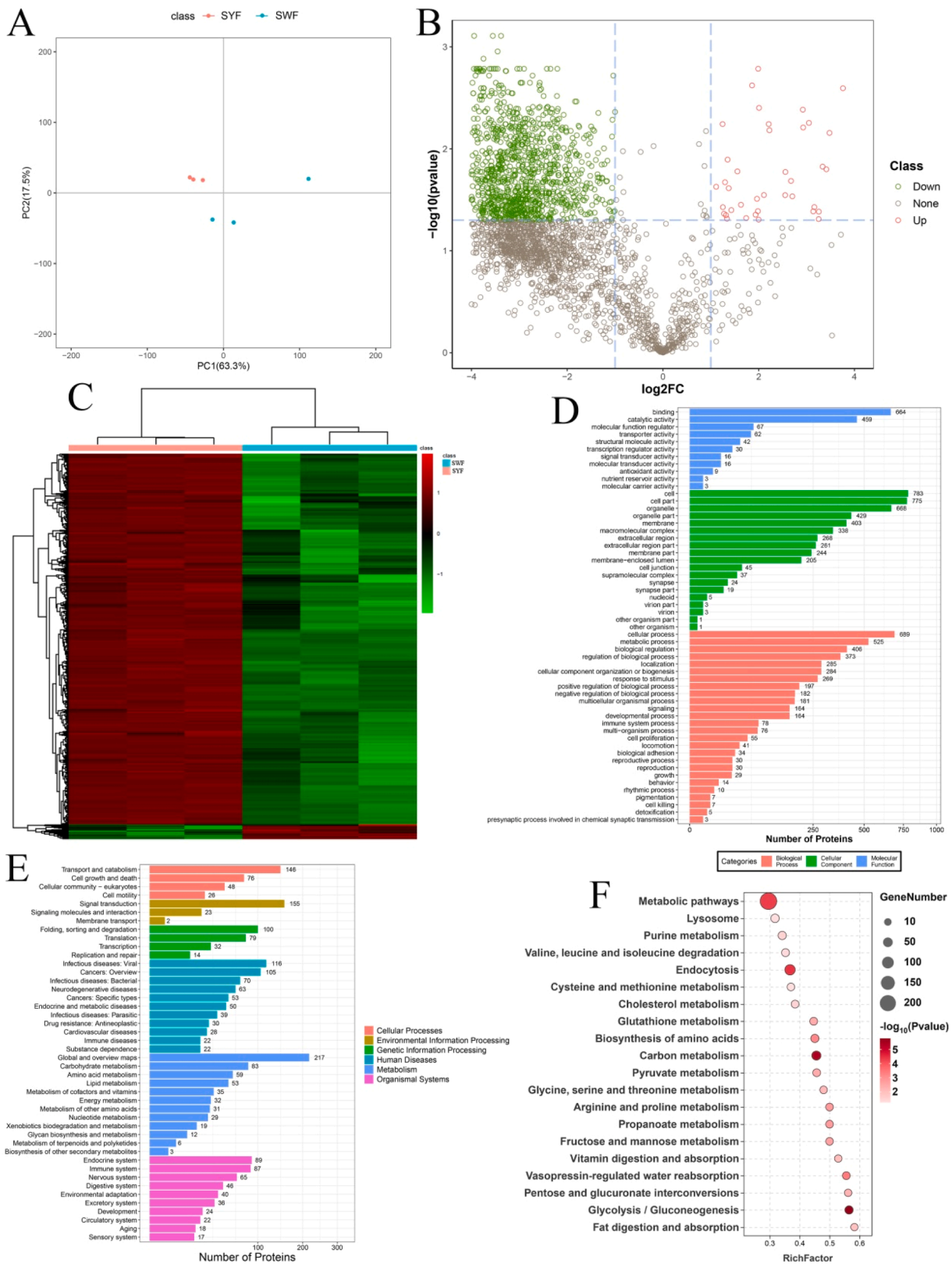

Fig. 4. Identification and functional enrichment analysis of DEPs. (A) Principal component analysis (PCA) distribution of SWF and SYF samples. (B) 1276 DEPs (48 upregulated and 1228 downregulated) were presented in a volcano plot. (C) The hierarchical cluster analysis of DEPs. (D) The significance GO terms of biological process, cellular component, and molecular function of DEPs. (E) KEGG pathway annotation. The KEGG metabolic pathway is divided into seven branches: Cellular Processes, Environmental Information Processing, Genetic Information Processing, Human disease Diseases (animals only), Metabolism, Organismal Systems, and Drug Development. (F) Top 20 significantly changed pathways associated with DEPs.

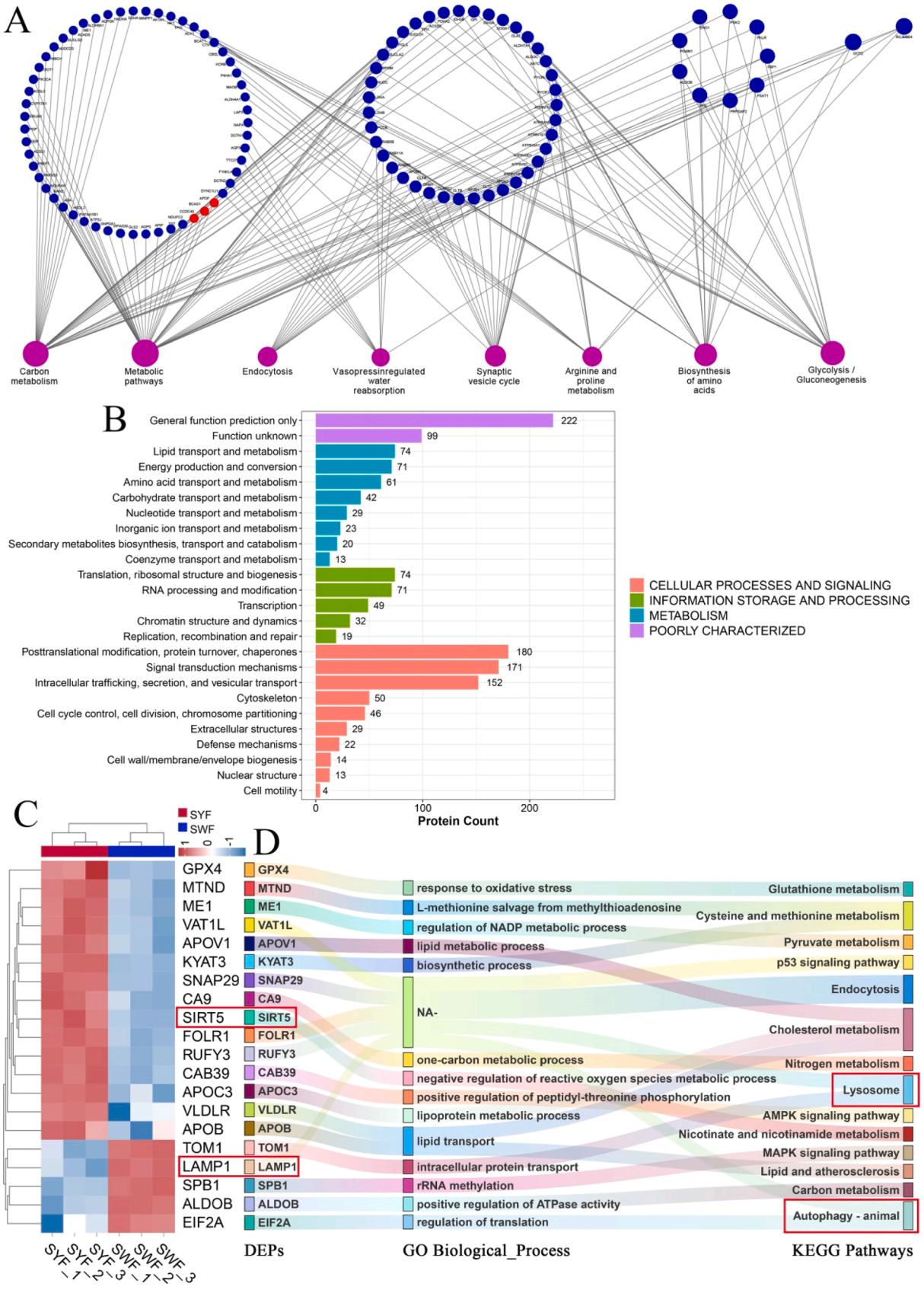

Fig. 5. Pathway relationship networks, KOG annotation, and functional analysis of DEPs. (A) Pathway relationship networks of DEPs. (B) KOG annotation of DEPs. (C) Hierarchical clustering analysis and functional enrichment analysis of the top 20 highly DEPs.

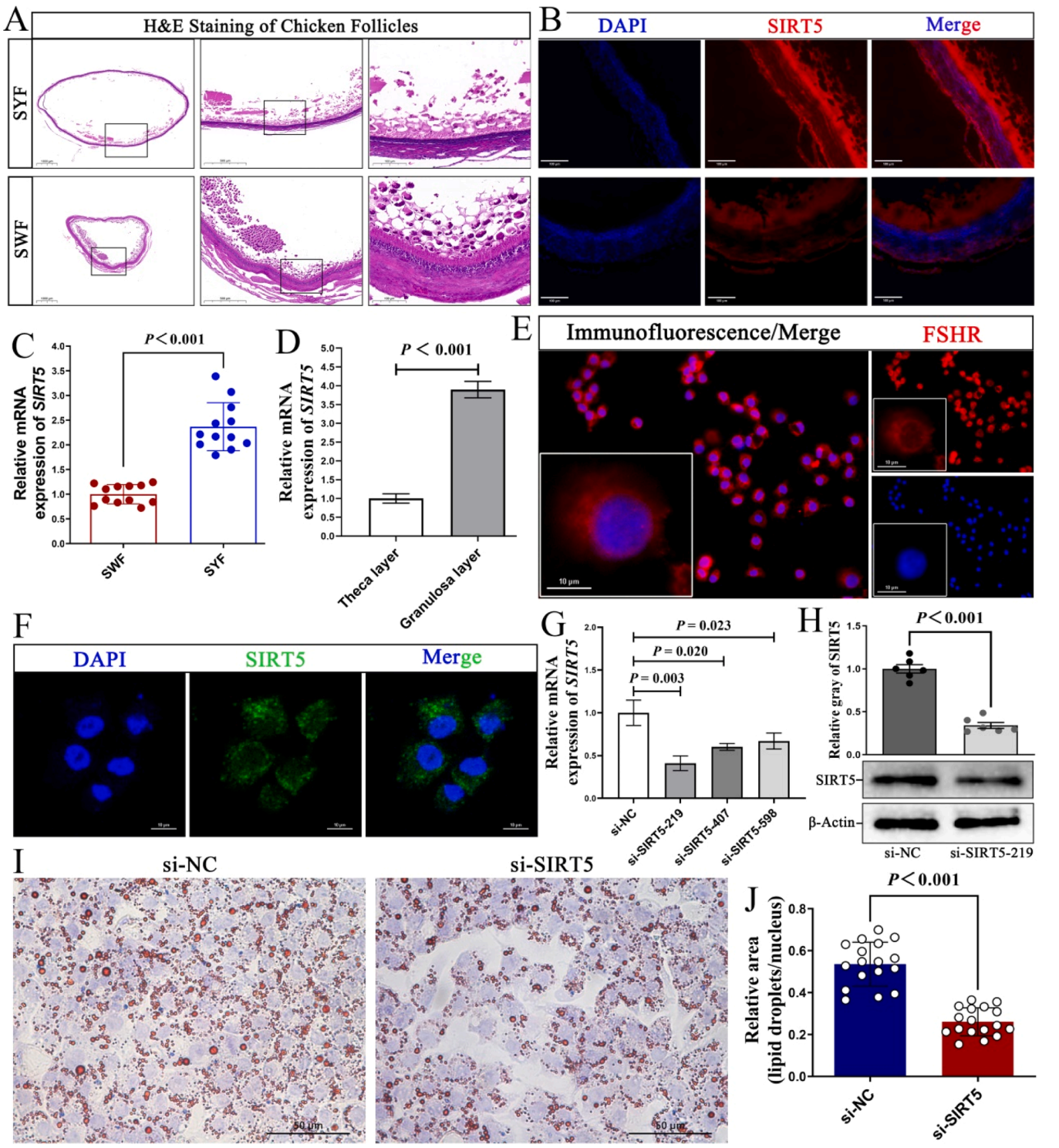

Fig. 6. The expression of SIRT5 in chicken SWF, SYF and GCs. (A) The H&E staining of SYF and SWF. (B) The immunofluorescence analysis of SIRT5 in SYF and SWF. (C) The mRNA expression of SIRT5 in SYF and SWF, (D) and in granulosa layer and theca layer. (E) The identification of the GCs by using FSHR immunofluorescence assay. (F) The immunofluorescence assay of SIRT5 in GCs. (G) The mRNA expression of SIRT5 was detected after transfection of small RNA interference (si-RNA) in GCs. (H) The protein expression of SIRT5 after the transfection of si-SIRT5-219 in the GCs. (I and J) The deposition of lipid droplets in the GCs after the transfection of si-SIRT5-219.

and the results showed that SIRT5 was highly and mainly expressed in cytoplasm of GCs (Fig. 6F). Three small RNA interference (si-SIRT5-219, si-SIRT5-407, and si-SIRT5-598) were used to knockdown SIRT5 expression, and the results showed that this three interfering vectors reduced the mRNA expression of SIRT5 in different degrees and si-SIRT5-219 has the highest inhibition efficiency (Fig. 6G), and the protein expression of SIRT5 was significantly reduced after the transfection of si-SIRT5-219 in the GCs (Fig. 6H), which subsequently decrease the deposition of lipid droplets in the GCs (Fig. 6I and J).

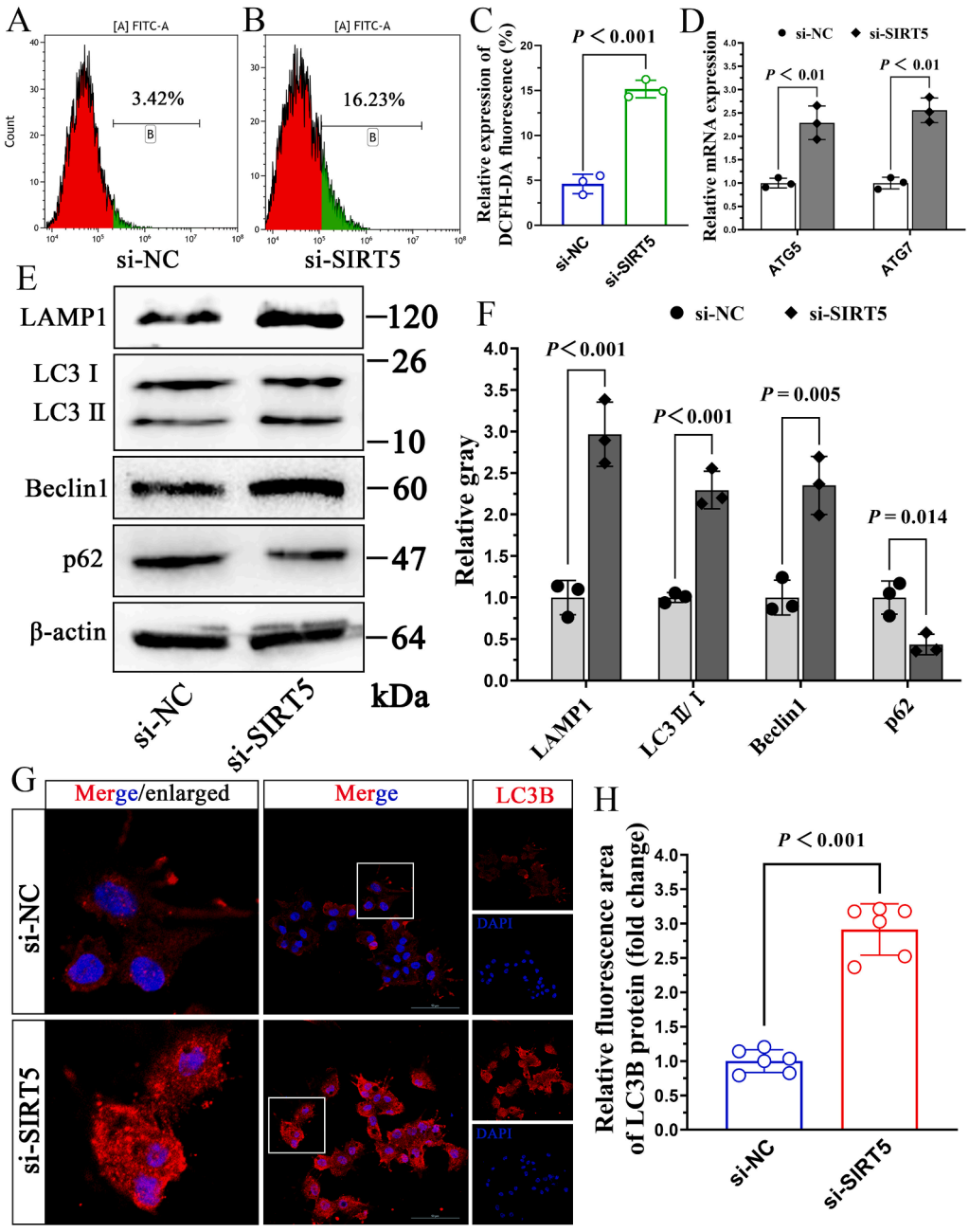

Fig. 7. SIRT5 regulated the autophagy of GCs. (A, B and C) The determination of the ROS level. (D) The mRNA expression of autophagy-related genes after a transfection of SIRT5 inhibition. (E and F) The protein expression level of autophagy-related proteins after a transfection of SIRT5 inhibition. (G and H) The immunofluorescence assay of LC3B after SIRT5 inhibition in GCs.

SIRT5 silence increased the production of ROS and promoted autophagy of GCs

SIRT5 regulates ROS production and autophagy in severer cell types (Fiorentino et al., 2022; Jung et al., 2022; Barreca et al., 2023; Deng et al., 2024), hence, we further assessed the ROS levels in the GCs after silencing *SIRT5*. The results showed that SIRT5 knockdown significantly increased ROS production in GCs compared with the si-NC group (Fig. 7A–C). Moreover, after a transfection of *SIRT5* inhibition, the mRNA expression of autophagy-related genes *ATG5* and *ATG7* were significantly increased (Fig. 7D), and the protein expression level of the autophagy marker proteins, such as LC3-II/I (Microtubule Associated Protein Light Chain 3B) and Beclin1, and the markers of lysosome LAMP1 were significantly increased, whereas the expression of p62 was significantly decreased (degrade) compared with the si-NC group (Fig. 7E and F). The immunofluorescence assay of LC3B in GCs showed significantly increased fluorescent intensity after SIRT5 silencing, confirming that SIRT5 inhibits autophagy in GCs (Fig. 7G and H).

Discussion

Cyclic follicle recruitment is a vital stage in the development of poultry follicles, playing a significant role in determining egg-laying performance (Ghanem and Johnson, 2019a; Ghanem and Johnson, 2019b; Ghanem and Johnson, 2021). Failure in this process results in follicular atresia, as evidenced by an accumulation of atrophic follicles in chicken ovaries during the late laying period, which severely limits egg production (Liu et al., 2018; Cui et al., 2020b; Xiong et al., 2024; Yu

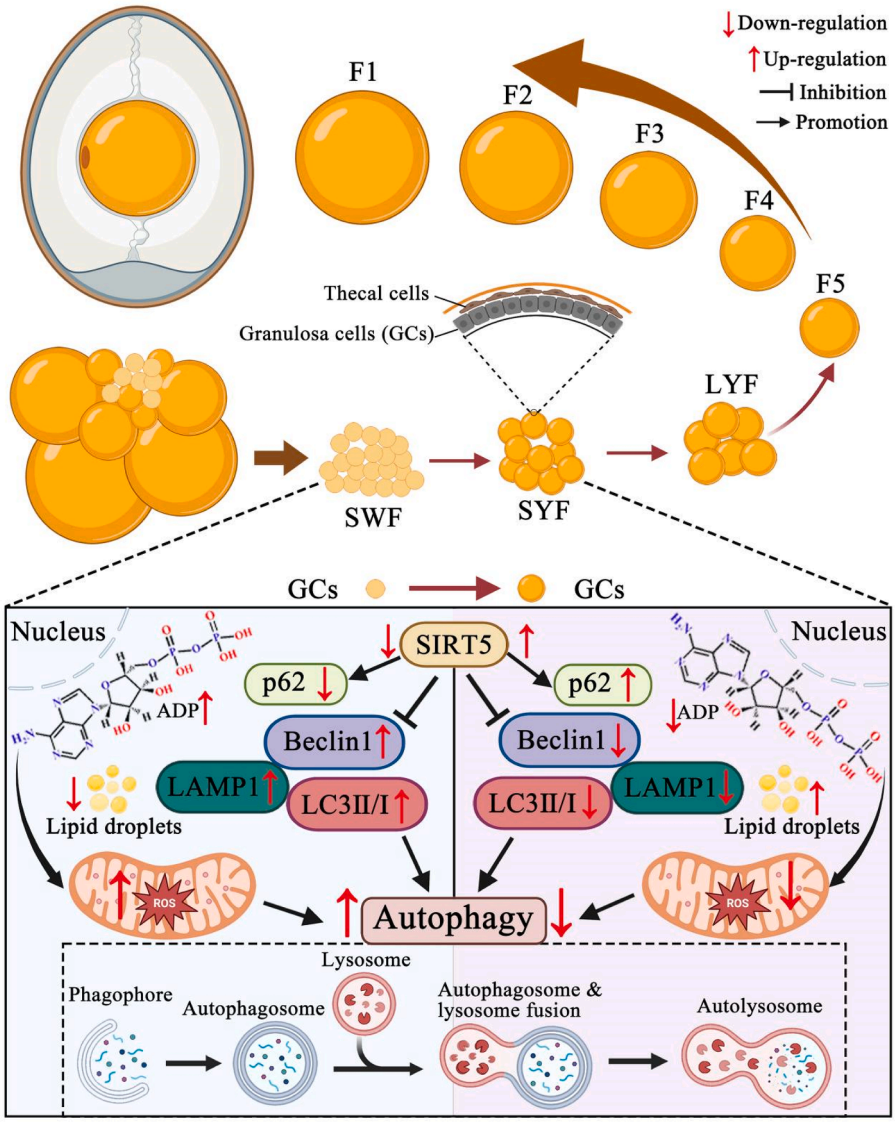

Fig. 8. Schematic model illustrates the role of Sirtuin 5 (SIRT5) in the regulation of follicular recruitment in chickens through its influence on the autophagy-lysosome pathway in granulosa cells (GCs). The upregulation of SIRT5 inhibits excessive autophagy, stabilize mitochondrial activity, reduce oxidative stress, and enhance lipid droplet formation, which contribute to the promotion of follicular recruitment in chickens. This provides insights into the molecular control of reproductive processes in chickens.

et al., 2024). In this present study, we used integrated proteomic and metabolomic analyses to investigate follicular recruitment in chickens, and it was revealed that DMs were enriched in pathways such as Lysosome, Ferroptosis, Insulin signaling pathway, Biosynthesis of unsaturated fatty acids, Tryptophan metabolism, etc., and DEPs were enriched in Lysosome, Glutathione metabolism, Cholesterol metabolism, Arginine and proline metabolism, Biosynthesis of amino acids. Both DMs and DEPs were enriched in the Lysosome pathway, which was identified as essential in regulating ovulation in chickens (Nie et al., 2024), and associated with follicular atresia in geese (Yang et al., 2023). A study by Han, et al reported that activation of ferroptosis in chicken GCs has been linked to follicular atresia (Han et al., 2024), as well as reported in geese (Zhang et al., 2024). Lysosomes act as cellular degradation centers and signaling hubs, playing an essential role in maintaining cellular homeostasis (Yang and Wang, 2021). They regulate autophagy and autophagic cell death (Mahapatra et al., 2021) by degrading cytoplasmic components, including damaged organelles (Nixon and Rubinsztein, 2024). In this study, SIRT5 was found to be significantly upregulated, while lysosomal-associated membrane protein 1 (LAMP1) was down-regulated during chicken pre-recruitment follicle development. SIRT5 negatively regulated reactive oxygen species metabolism, whereas LAMP1 and Adenosine 5'-Diphosphate (ADP) were enriched in lysosome and autophagy pathways. Moreover, Adenosine 5′-Diphosphate (ADP) was downregulated and significantly enriched in Lysosome pathway. Previous research has demonstrated that SIRT5 regulates ROS level and autophagy across various cell types (Singh et al., 2018; Barreca et al., 2023). In addition, other reports indicated that SIRT5 activation controls ammonia-induced autophagy and mitophagy (Polletta et al., 2015), mitigates apoptosis and autophagy in bovine mammary epithelial cells (He et al., 2024b), reduces cancer cell vitality by modulating autophagy, mitophagy and ROS (Barreca et al., 2023), and supports lipid metabolism (Hong et al., 2020; Wu et al., 2024). Consistently, it was revealed in this study that SIRT5 deficiency in GCs promoted ROS production and inhibited lipid synthesis. These results were consistent with the findings of previous studies that reported that SIRT5 promotes lipid synthesis and inhibits ROS concentration. Moreover, elevated ADP levels have also been linked to ROS production (Ramzan et al., 2022; Skulachev et al., 2023), which further induced autophagy (Park and

Chung, 2019; Wang et al., 2022). In this present study, ADP levels were higher in SWF than in SYF, while SIRT5 expression was lower in SWF than in SYF. Silencing SIRT5 in GCs led to increased ROS production and autophagy. These findings align with previous research showing that reported that an increased ADP level can induce autophagy in mesenchymal stem cells (Zhang et al., 2022), promote lysosomal exocytosis (Södergren et al., 2016).

LAMP1 and LC3B (microtubule-associated proteins 1 light chain 3 beta, LC3II) are recognized markers for lysosomes (Zhang et al., 2023) and autophagosomes (Zhan et al., 2022), respectively. In this study, both LAMP1 and ADP were downregulated during the development of pre-recruitment follicles and enriched in the Lysosome pathway. LAMP1 is a standard lysosome marker (Cheng et al., 2018), while ADP has been shown to restore lysosomal exocytosis (Sharda et al., 2015). Silencing SIRT5 increased the expression of autophagy-related proteins. Such as LC3II and Beclin1, as well as the lysosome marker LAMP1, while reducing lipid droplet accumulation and p62 expression. These findings indicate that up-regulated SIRT5 during the development of chicken pre-recruitment follicles suppresses GCs autophagy by inhibiting LAMP1 expression and reducing ADP and ROS levels. Supporting this, Garva, et al. (2019) reported that SIRT5 silencing enhances autophagy by increasing the LC3 II/I ratio and Beclin-1 protein levels (Garva et al., 2019). Salomone et al. (2024) found that SIRT5 inhibition elevates ADP levels in HepG2 cells (Salomone et al., 2024).

Conclusions

Taken together, this study revealed an increased yolk deposition during the development of chicken pre-recruitment follicles. Integrated proteomic and metabolomic analyses showed that SIRT5, a DEP, was significantly upregulated, while lysosomal-associated membrane protein 1 (LAMP1) and ADP, both enriched in lysosome and autophagy pathways, were downregulated. Silencing SIRT5 led to elevated ROS production, increased autophagy-related protein expression, and reduced lipid synthesis, highlighting the crucial role of SIRT5 in regulating ROS metabolism, autophagy, and lipid synthesis during the development of pre-recruitment follicles in chicken GCs (Fig. 8).

Declaration of competing interest

The authors declare no competing financial interest.

Acknowledgments

This study was supported by the Natural Science Foundation of Chongqing (CSTB2023NSCQ-MSX1184), National Key Research and Development Program of China (2023YFF1103802), the Fundamental Research Funds for the Central Universities (SWU-KQ22080), and the Chongqing Modern Agricultural Industry Technology System (Poultry) (CQMAITS202314-3).

Supplementary materials

Supplementary material associated with this article can be found, in the online version, at doi:10.1016/j.psj.2025.104884.

References

Barreca, F., Aventaggiato, M., Vitiello, L., Sansone, L., Russo, M.A., Mai, A., Valente, S., Tafani, M., 2023. SIRT5 Activation and inorganic phosphate binding reduce cancer cell vitality by modulating autophagy/mitophagy and ROS. Antioxidants (Basel, Switzerland) 12, 1635.

Bruderer, R., Bernhardt, O.M., Gandhi, T., Miladinović, S.M., Cheng, L.Y., Messner, S., Ehrenberger, T., Zanotelli, V., Butscheid, Y., Escher, C., Vitek, O., Rinner, O., Reiter, L., 2015. Extending the limits of quantitative proteome profiling with data-independent acquisition and application to acetaminophen-treated three-dimensional liver microtissues. Mol. Cell. Proteomics 14, 1400–1410.

Cheng, X.T., Xie, Y.X., Zhou, B., Huang, N., Farfel-Becker, T., Sheng, Z.H., 2018. Revisiting LAMP1 as a marker for degradative autophagy-lysosomal organelles in the nervous system. Autophagy 14, 1472–1474.

Choi, M., Chang, C.Y., Clough, T., Broudy, D., Killeen, T., MacLean, B., Vitek, O., 2014. MSstats: an R package for statistical analysis of quantitative mass spectrometry-based proteomic experiments. Bioinformatics 30, 2524–2526.

Cox, J., Mann, M., 2008. MaxQuant enables high peptide identification rates, individualized p.p.b.-range mass accuracies and proteome-wide protein quantification. Nat. Biotechnol. 26, 1367–1372.

Cui, Z., Amevor, F.K., Feng, Q., Kang, X., Song, W., Zhu, Q., Wang, Y., Li, D., Zhao, X., 2020a. Sexual maturity promotes yolk precursor synthesis and follicle development in hens via liver-blood-ovary signal axis. Animals 10, 2348.

Cui, Z., Liu, L., Kwame Amevor, F., Zhu, Q., Wang, Y., Li, D., Shu, G., Tian, Y., Zhao, X., 2020b. High expression of miR-204 in chicken atrophic ovaries promotes granulosa cell apoptosis and inhibits autophagy. Front. Cell Dev. Biol. 8, 580072.

Cui, Z., Ning, Z., Deng, X., Du, X., Amevor, F.K., Liu, L., Kang, X., Tian, Y., Wang, Y., Li, D., Zhao, X., 2022. Integrated proteomic and metabolomic analyses of chicken ovary revealed the crucial role of lipoprotein lipase on lipid metabolism and steroidogenesis during sexual maturity. Front. Physiol. 13, 885030.

Cui, Z., Shen, X., Zhang, X., Li, F., Amevor, F.K., Zhu, Q., Wang, Y., Li, D., Shu, G., Tian, Y., Zhao, X., 2021. A functional polymorphism of inhibin alpha subunit at miR-181b-1-3p-binding site regulates proliferation and apoptosis of chicken ovarian granular cells. Cell Tissue Res. 384, 545–560.

Deng, P., Fan, T., Gao, P., Peng, Y., Li, M., Li, J., Qin, M., Hao, R., Wang, L., Li, M., Zhang, L., Chen, C., He, M., Lu, Y., Ma, Q., Luo, Y., Tian, L., Xie, J., Chen, M., Xu, S., Zhou, Z., Yu, Z., Pi, H., 2024. SIRT5-Mediated desuccinylation of RAB7A protects against cadmium-induced Alzheimer's disease-like pathology by restoring autophagic flux. Adv. Sci. (Weinheim, Baden-Wurttemberg, Germany) 11, e2402030.

Dong, J., Guo, C., Zhou, S., Zhao, A., Li, J., Mi, Y., Zhang, C., 2022. Leukemia inhibitory factor prevents chicken follicular atresia through PI3K/AKT and Stat3 signaling pathways. Mol. Cell Endocrinol. 543, 111550.

Etches, R.J., Petitte, J.N., 1990. Reptilian and avian follicular hierarchies: models for the study of ovarian development. J. Exp. Zool. Suppl. 4, 112–122.

Fiorentino, F., Castiello, C., Mai, A., Rotili, D., 2022. Therapeutic potential and activity modulation of the protein lysine deacylase sirtuin 5. J. Med. Chem. 65, 9580–9606.

Fiorentino, G., Cimadomo, D., Innocenti, F., Soscia, D., Vaiarelli, A., Ubaldi, F.M., Gennarelli, G., Garagna, S., Rienzi, L., Zuccotti, M., 2023. Biomechanical forces and signals operating in the ovary during folliculogenesis and their dysregulation: implications for fertility. Hum. Reprod. Update 29, 1–23.

Garva, R., Thepmalee, C., Yasamut, U., Sudsaward, S., Guazzelli, A., Rajendran, R., Tongmuang, N., Khunchai, S., Meysami, P., Limjindaporn, T., Yenchitsomanus, P.T., Mutti, L., Krstic-Demonacos, M., Demonacos, C., 2019. Sirtuin Family members selectively regulate autophagy in osteosarcoma and mesothelioma cells in response to cellular stress. Front. Oncol. 9, 949.

Ghanem, K., Johnson, A.L., 2019a. Relationship between cyclic follicle recruitment and ovulation in the hen ovary. Poult. Sci. 98, 3014–3021.

Ghanem, K., Johnson, A.L., 2019b. Response of hen pre-recruitment ovarian follicles to follicle stimulating hormone, in vivo. Gen. Comp. Endocrinol. 270, 41–47.

Ghanem, K., Johnson, A.L., 2021. Proteome profiling of chicken ovarian follicles immediately before and after cyclic recruitment. Mol. Reprod. Dev. 88, 571–583.

Gilbert, A.B., Evans, A.J., Perry, M.M., Davidson, M.H., 1977. A method for separating the granulosa cells, the basal lamina and the theca of the preovulatory ovarian follicle of the domestic fowl (Gallus domesticus). J. Reprod. Fertil. 50, 179–181.

Gilbert, A.B., Perry, M.M., Waddington, D., Hardie, M.A., 1983. Role of atresia in establishing the follicular hierarchy in the ovary of the domestic hen (Gallus domesticus). J. Reprod. Fertil. 69, 221–227.

Guiné, R.P.F., 2024. The challenges and strategies of food security under global change. Foods (Basel, Switzerland) 13, 2083.

Han, S., Wang, J., Cui, C., Yu, C., Zhang, Y., Li, D., Ma, M., Du, H., Jiang, X., Zhu, Q., Yang, C., Yin, H., 2022. Fibromodulin is involved in autophagy and apoptosis of granulosa cells affecting the follicular atresia in chicken. Poult. Sci. 101, 101524.

Han, S., Yu, C., Qiu, M., Xiong, X., Peng, H., Song, X., Hu, C., Zhang, Z., Xia, B., Yang, L., Chen, J., Zhu, S., Li, W., Yang, C., 2024. USP13 regulates ferroptosis in chicken follicle granulosa cells by deubiquitinating ATG7. Poult. Sci. 103, 104209.

Han, S., Zhao, X., Zhang, Y., Amevor, F.K., Tan, B., Ma, M., Kang, H., Wang, J., Zhu, Q., Yin, H., Cui, C., 2023. MiR-34a-5p promotes autophagy and apoptosis of ovarian granulosa cells via the Hippo-YAP signaling pathway by targeting LEF1 in chicken. Poult. Sci. 102, 102374.

He, H., Li, D., Tian, Y., Wei, Q., Amevor, F.K., Sun, C., Yu, C., Yang, C., Du, H., Jiang, X., Ma, M., Cui, C., Zhang, Z., Tian, K., Zhang, Y., Zhu, Q., Yin, H., 2022. miRNA sequencing analysis of healthy and atretic follicles of chickens revealed that miR-30a-5p inhibits granulosa cell death via targeting Beclin1. J. Anim. Sci. Biotechnol. 13, 55.

He, H., Wei, Y., Chen, Y., Zhao, X., Shen, X., Zhu, Q., Yin, H., 2024a. High expression circRALGPS2 in atretic follicle induces chicken granulosa cell apoptosis and autophagy via encoding a new protein. J. Anim. Sci. Biotechnol. 15, 42.

He, J., Feng, L., Yang, H., Gao, S., Dong, J., Lu, G., Liu, L., Zhang, X., Zhong, K., Guo, S., Zha, G., Han, L., Li, H., Wang, Y., 2024b. Sirtuin 5 alleviates apoptosis and autophagy stimulated by ammonium chloride in bovine mammary epithelial cells. Exp. Ther. Med. 28, 295.

Hong, J., Mei, C., Raza, S.H.A., Khan, R., Cheng, G., Zan, L., 2020. SIRT5 inhibits bovine preadipocyte differentiation and lipid deposition by activating AMPK and repressing MAPK signal pathways. Genomics 112, 1065–1076.

Hussein, M.R., 2005. Apoptosis in the ovary: molecular mechanisms. Hum. Reprod. Update 11, 162–177.

Johnson, Alan, L., 2014. The avian ovary and follicle development: some comparative and practical insights. Turk. J. Vet. Anim. Sci. 38, 660–669.
Johnson, A.L., 2015a. Ovarian follicle selection and granulosa cell differentiation. Poult. Sci. 94, 781–785.
Johnson, A.L., 2015b. Reproduction in the Female. Sturkie's Avian Physiology, Sixth Edition, pp. 635–665.
Johnson, A.L., Woods, D.C., 2009. Dynamics of avian ovarian follicle development: cellular mechanisms of granulosa cell differentiation. Gen. Comp. Endocrinol. 163, 12–17.
Johnson, P.A., Stephens, C.S., Giles, J.R., 2015. The domestic chicken: causes and consequences of an egg a day. Poult. Sci. 94, 816–820.
Jung, Y.H., Chae, C.W., Chang, H.S., Choi, G.E., Lee, H.J., Han, H.J., 2022. Silencing SIRT5 induces the senescence of UCB-MSCs exposed to TNF-α by reduction of fatty acid β-oxidation and anti-oxidation. Free Radic Biol. Med. 192, 1–12.
Kim, D., Johnson, A.L., 2016. Vasoactive intestinal peptide promotes differentiation and clock gene expression in granulosa cells from prehierarchal follicles. Mol. Reprod. Dev. 83, 455–463.
Li, D., Ning, C., Zhang, J., Wang, Y., Tang, Q., Kui, H., Wang, T., He, M., Jin, L., Li, J., Lin, Y., Zeng, B., Yin, H., Zhao, X., Zhang, Y., Xu, H., Zhu, Q., Li, M., 2022. Dynamic transcriptome and chromatin architecture in granulosa cells during chicken folliculogenesis. Nat. Commun. 13, 131.
Li, Q., Hu, S., Wang, Y., Deng, Y., Yang, S., Hu, J., Li, L., Wang, J., 2019. mRNA and miRNA transcriptome profiling of granulosa and theca layers from geese ovarian follicles reveals the crucial pathways and interaction networks for regulation of follicle selection. Front. Genet. 10, 988.
Liu, L., Xiao, Q., Gilbert, E.R., Cui, Z., Zhao, X., Wang, Y., Yin, H., Li, D., Zhang, H., Zhu, Q., 2018. Whole-transcriptome analysis of atrophic ovaries in broody chickens reveals regulatory pathways associated with proliferation and apoptosis. Sci. Rep. 8, 7231.
Livak, K.J., Schmittgen, T.D., 2001. Analysis of relative gene expression data using real-time quantitative PCR and the 2(-Delta Delta C(T)) method. Methods 25, 402–408.
Mahapatra, K.K., Mishra, S.R., Behera, B.P., Patil, S., Gewirtz, D.A., Bhutia, S.K., 2021. The lysosome as an imperative regulator of autophagy and cell death. Cell Mol. Life Sci. 78, 7435–7449.
McGee, E.A., Hsueh, A.J., 2000. Initial and cyclic recruitment of ovarian follicles. Endocr. Rev. 21, 200–214.
Nie, R., Zhang, W., Tian, H., Li, J., Ling, Y., Zhang, B., Zhang, H., Wu, C., 2024. Proteo-transcriptomic profiles reveal key regulatory pathways and functions of LDHA in the ovulation of domestic chickens (Gallus gallus). J. Anim. Sci. Biotechnol. 15, 68.
Ning, Z., Deng, X., Li, L., Feng, J., Du, X., Amevor, F.K., Tian, Y., Li, L., Rao, Y., Yi, Z., Du, X., Cui, Z., Zhao, X., 2023. miR-128-3p regulates chicken granulosa cell function via 14-3-3β/FoxO and PPAR-γ/LPL signaling pathways. Int. J. Biol. Macromol. 241, 124654.
Nishio, N., Isobe, K.I., 2023. Hen egg only diets support healthy aging in adult mice. J. Anim. Physiol. Anim. Nutr. 107, 1110–1124.
Nixon, R.A., Rubinsztein, D.C., 2024. Mechanisms of autophagy-lysosome dysfunction in neurodegenerative diseases. Nat. Rev. Mol. Cell Biol. 25, 926–946.
Ocłoń, E., Hrabia, A., 2021. miRNA expression profile in chicken ovarian follicles throughout development and miRNA-mediated MMP expression. Theriogenology 160, 116–127.
Onagbesan, O., Bruggeman, V., Decuypere, E., 2009. Intra-ovarian growth factors regulating ovarian function in avian species: a review. Anim. Reprod. Sci. 111, 121–140.
Park, E., Chung, S.W., 2019. ROS-mediated autophagy increases intracellular iron levels and ferroptosis by ferritin and transferrin receptor regulation. Cell Death. Dis. 10, 822.
Polletta, L., Vernucci, E., Carnevale, I., Arcangeli, T., Rotili, D., Palmerio, S., Steegborn, C., Nowak, T., Schutkowski, M., Pellegrini, L., Sansone, L., Villanova, L., Runci, A., Pucci, B., Morgante, E., Fini, M., Mai, A., Russo, M.A., Tafani, M., 2015. SIRT5 regulation of ammonia-induced autophagy and mitophagy. Autophagy 11, 253–270.
Ramzan, R., Dolga, A.M., Michels, S., Weber, P., Culmsee, C., Rastan, A.J., Vogt, S., 2022. Cytochrome c oxidase inhibition by ATP decreases mitochondrial ROS production. Cells 11, 992.
Rolaki, A., Drakakis, P., Millingos, S., Loutradis, D., Makrigiannakis, A., 2005. Novel trends in follicular development, atresia and corpus luteum regression: a role for apoptosis. Reprod. Biomed. Online 11, 93–103.
Salomone, F., Pipitone, R.M., Longo, M., Malvestiti, F., Amorini, A.M., Distefano, A., Casirati, E., Ciociola, E., Iraci, N., Leggio, L., Zito, R., Vicario, N., Saoca, C., Pennisi, G., Cabibi, D., Lazzarino, G., Fracanzani, A.L., Dongiovanni, P., Valenti, L., Petta, S., Volti, G.L., Grimaudo, S., 2024. SIRT5 rs12216101 T>G variant is associated with liver damage and mitochondrial dysfunction in patients with non-alcoholic fatty liver disease. J. Hepatol. 80, 10–19.
Sasanami, T., 2017. Avian reproduction: from behavior to molecules. Adv. Exp. Med. Biol. http://www.springer.com/series/5584.
Shakoor, H., Khan, M.I., Sahar, A., Khan, M.K.I., Faiz, F., Ahmad, H.Basheer, 2020. Development of omega-3 rich eggs through dietary flaxseed and bio-evaluation in metabolic syndrome. Food Sci. Nutr. 8, 2619–2626.
Shao, T., Ke, H., Liu, R., Xu, L., Han, S., Zhang, X., Dang, Y., Jiao, X., Li, W., Chen, Z.J., Qin, Y., Zhao, S., 2022. Autophagy regulates differentiation of ovarian granulosa cells through degradation of WT1. Autophagy 18, 1864–1878.
Sharda, A., Kim, S.H., Jasuja, R., Gopal, S., Flaumenhaft, R., Furie, B.C., Furie, B., 2015. Defective PDI release from platelets and endothelial cells impairs thrombus formation in Hermansky-Pudlak syndrome. Blood 125, 1633–1642.
Singh, C.K., Chhabra, G., Ndiaye, M.A., Garcia-Peterson, L.M., Mack, N.J., Ahmad, N., 2018. The role of sirtuins in antioxidant and redox signaling. Antioxid. Redox Signal. 28, 643–661.
Skulachev, V.P., Vyssokikh, M.Y., Chernyak, B.V., Mulkidjanian, A.Y., Skulachev, M.V., Shilovsky, G.A., Lyamzaev, K.G., Borisov, V.B., Severin, F.F., Sadovnichii, V.A., 2023. Six functions of respiration: isn't it time to take control over ROS production in mitochondria, and aging along with it? Int. J. Mol. Sci. 24, 12540.
Södergren, A.L., Svensson Holm, A.C., Ramström, S., Lindström, E.G., Grenegård, M., Öllinger, K., 2016. Thrombin-induced lysosomal exocytosis in human platelets is dependent on secondary activation by ADP and regulated by endothelial-derived substances. Platelets. 27, 86–92.
Soliman, G.A., 2018. Dietary cholesterol and the lack of evidence in cardiovascular disease. Nutrients 10, 780.
Sun, T., Xiao, C., Yang, Z., Deng, J., Yang, X., 2022. Grade follicles transcriptional profiling analysis in different laying stages in chicken. Bmc Genomics [Electronic Resource] 23, 492.
Sun, X., Chen, X., Zhao, J., Ma, C., Yan, C., Liswaniso, S., Xu, R., Qin, N., 2021. Transcriptome comparative analysis of ovarian follicles reveals the key genes and signaling pathways implicated in hen egg production. Bmc Genomics [Electronic Resource] 22, 899.
Wang, J., Yue, H., Wu, S., Zhang, H., Qi, G., 2017a. Nutritional modulation of health, egg quality and environmental pollution of the layers. Anim. Nutr. (Zhongguo xu mu shou yi xue hui) 3, 91–96.
Wang, Y., Chen, Q., Liu, Z., Guo, X., Du, Y., Yuan, Z., Guo, M., Kang, L., Sun, Y., Jiang, Y., 2017b. Transcriptome analysis on single small yellow follicles reveals that Wnt4 is involved in chicken follicle selection. Front. Endocrinol. 8, 317.
Wang, Y.T., Liu, T.Y., Shen, C.H., Lin, S.Y., Hung, C.C., Hsu, L.C., Chen, G.C., 2022. K48/K63-linked polyubiquitination of ATG9A by TRAF6 E3 ligase regulates oxidative stress-induced autophagy. Cell Rep. 38, 110354.
Want, E.J., Masson, P., Michopoulos, F., Wilson, I.D., Theodoridis, G., Plumb, R.S., Shockcor, J., Loftus, N., Holmes, E., Nicholson, J.K., 2013. Global metabolic profiling of animal and human tissues via UPLC-MS. Nat. Protoc. 8, 17–32.
Wu, M., Tan, J., Cao, Z., Cai, Y., Huang, Z., Chen, Z., He, W., Liu, X., Jiang, Y., Gao, Q., Deng, B., Wang, J., Yuan, W., Zhang, H., Chen, Y., 2024. Sirt5 improves cardiomyocytes fatty acid metabolism and ameliorates cardiac lipotoxicity in diabetic cardiomyopathy via CPT2 de-succinylation. Redox. Biol. 73, 103184.
Xiong, H., Li, W., Wang, L., Wang, X., Tang, B., Cui, Z., Liu, L., 2024. Whole transcriptome analysis revealed the regulatory network and related pathways of non-coding RNA regulating ovarian atrophy in broody hens. Front. Vet. Sci. 11, 1399776.
Yang, C., Wang, X., 2021. Lysosome biogenesis: regulation and functions. J. Cell Biol. 220, e202102001.
Yang, W., Chen, X., Liu, Z., Zhao, Y., Chen, Y., Geng, Z., 2023. Integrated transcriptome and proteome revealed that the declined expression of cell cycle-related genes associated with follicular atresia in geese. Bmc Genomics [Electronic Resource] 24, 24.
Yu, C., Lin, Z., Song, X., Hu, C., Qiu, M., Yang, L., Zhang, Z., Pen, H., Chen, J., Xiong, X., Xia, B., Jiang, X., Du, H., Li, Q., Zhu, S., Liu, S., Yang, C., Liu, Y., 2022. Whole transcriptome analysis reveals the key genes and noncoding RNAs related to follicular atresia in broilers. Anim. Biotechnol. 34, 3144–3153.
Yu, C., Qiu, M., Xiong, X., Peng, H., Han, S., Song, X., Hu, C., Zhang, Z., Xia, B., Chen, J., Zhu, S., Yang, L., Li, W., Yin, H., Zhao, J., Lin, Z., Liu, Y., Yang, C., 2024. Integrative analysis of RNA-seq and ribo-seq reveals that lncRNA-GRN regulates chicken follicular atresia through miR-103-3p/FBXW7 axis and encoding peptide. Int. J. Biol. Macromol. 278, 135051.
Yu, J., He, K., Ren, T., Lou, Y., Zhao, A., 2016. High-throughput sequencing reveals differential expression of miRNAs in prehierarchal follicles of laying and brooding geese. Physiol. Genomics 48, 455–463.
Yu, Y.S., Sui, H.S., Han, Z.B., Li, W., Luo, M.J., Tan, J.H., 2004. Apoptosis in granulosa cells during follicular atresia: relationship with steroids and insulin-like growth factors. Cell Res. 14, 341–346.
Zhan, Q., Jeon, J., Li, Y., Huang, Y., Xiong, J., Wang, Q., Xu, T.L., Li, Y., Ji, F.H., Du, G., Zhu, M.X., 2022. CAMK2/CaMKII activates MLKL in short-term starvation to facilitate autophagic flux. Autophagy 18, 726–744.
Zhang, J., Zeng, W., Han, Y., Lee, W.R., Liou, J., Jiang, Y., 2023. Lysosomal LAMP proteins regulate lysosomal pH by direct inhibition of the TMEM175 channel. Mol. Cell 83, 2524–2539 e2527.
Zhang, S., Xie, Y., Yan, F., Zhang, Y., Yang, Z., Chen, Z., Zhao, Y., Huang, Z., Cai, L., Deng, Z., 2022. Negative pressure wound therapy improves bone regeneration by promoting osteogenic differentiation via the AMPK-ULK1-autophagy axis. Autophagy 18, 2229–2245.
Zhang, Y., Jiang, Y., Dong, X., Luo, S., Jiao, G., Weng, K., Bao, Q., Zhang, Y., Vongsangnak, W., Chen, G., Xu, Q., 2024. Follicular fluid-derived exosomal HMOX1 promotes granulosa cell ferroptosis involved in follicular atresia in geese (Anser cygnoides). Poult. Sci. 103, 103912.
Zhou, S., Ma, Y., Zhao, D., Mi, Y., Zhang, C., 2020. Transcriptome profiling analysis of underlying regulation of growing follicle development in the chicken. Poult. Sci. 99, 2861–2872.